Absolute density and reaction kinetics of fluorine atoms in high-density c-C_4F_8 plasmas

K. Sasaki,[a] Y. Kawai, C. Suzuki, and K. Kadota
Department of Electronics, Nagoya University, Nagoya 464-8603, Japan

(Received 16 December 1997; accepted for publication 17 March 1998)

Absolute density and reaction kinetics of fluorine (F) atoms in high-density octafluorocyclobutane (c-C_4F_8) plasmas were examined using vacuum ultraviolet absorption spectroscopy. The F atom densities, corresponding to electron densities ranging from 1×10^{11} to 5×10^{12} cm^{-3}, were 1×10^{12}–5×10^{13} cm^{-3} for gas pressures of 2–7 mTorr and rf powers of 0.2–1.5 kW. The F atom density was linearly dependent on the electron density for $n_e<1.5\times10^{12}$ cm^{-3}. According to lifetime measurements in the afterglow, two decay processes were found in the F atom density: exponential (first-order kinetics) and linear (zero-order kinetics) decay components. The linear-decay component became significant at high gas pressures. The time constant of the exponential-decay component ranged from 5 to 100 ms, which corresponds to surface loss probabilities of 10^{-1}–10^{-3}. The surface loss probability varied inversely with the F atom density. © *1998 American Institute of Physics.* [S0021-8979(98)06112-X]

I. INTRODUCTION

Octafluorocyclobutane (c-C_4F_8, hereafter simply C_4F_8) plasmas are increasingly used in place of conventional CF_4 plasmas for selective dry etching of SiO_2 thin films over underlying Si in the fabrication of the ultralarge-scale integrated circuits.[1,2] Conventional CF_4 plasmas often result in poor etching selectivity of SiO_2 over Si when they are combined with low-pressure, high-density plasma sources[3,4] such as electron cyclotron resonance (ECR) plasmas, inductively coupled plasmas (ICPs), and helicon-wave excited plasmas. The etching selectivity can be improved considerably by using C_4F_8 instead of CF_4;[5,6] this is attributed to the high CF_x radial densities in C_4F_8 plasmas. One important aspect of SiO_2 etching with fluorocarbon plasmas is that the etching selectivity is sensitive to the density ratio of CF_x radicals to F atoms in the plasma.[6] This is because F atoms etch both Si and SiO_2, while CF_x radicals decrease the etching rate of Si by serving as precursors of polymerization. A number of works utilizing advanced diagnostics for CF_x radicals [e.g., infrared laser absorption spectroscopy (IRLAS),[7] appearance mass spectrometry (AMS),[8] and laser-induced fluorescence (LIF) spectroscopy[9,10]] show that the density of CF_x radicals is much higher in C_4F_8 plasmas than in CF_4 plasmas.[11–13] Absolute F atom densities in C_4F_8 plasmas have been difficult to investigate, however, due to the lack of reliable diagnostics. Although the actinometry technique[14] is extensively used for detecting F atoms, its reliability is doubtful in low-pressure, high-density plasmas.[15]

We recently measured the F atom density in a high-density helicon-wave CF_4 plasma using vacuum ultraviolet absorption spectroscopy (VUVAS).[16,17] This diagnostic is reliable and can yield the absolute F atom density with an error smaller than a factor of 2. In addition, the temporal variation of the F atom density in the afterglow can be observed by VUVAS. In a previous work,[16] lifetime measurements in the afterglow provided useful information on the loss processes of F atoms in a high-density CF_4 plasma. In the present work, we repeated the measurement in the same helicon-wave plasma source by replacing CF_4 with C $_4F_8$. The loss processes of F atoms in a high-density C_4F_8 plasma were examined again by lifetime measurements.

II. EXPERIMENT

The apparatus used in the present experiment is the same as that described in previous papers.[16,17] High-density plasmas were produced by helicon-wave discharges[18] in a linear machine with a uniform magnetic field of 1 kG. In the present work, we used pure C_4F_8 as the working gas in place of the CF_4 used in the previous experiment.[16] The vacuum chamber was composed of a Pyrex glass tube (9 cm in diameter) and two stainless-steel observation chambers ($20\times20\times10$ cm). Various rf powers from 0.2 to 1.5 kW were applied to a helical antenna wound around a quartz glass tube of 3 cm diam. The pressure range and the flow rate of the C_4F_8 gas were 1.5–7 mTorr and 1.6 ccm, respectively. The risk of breakdown in the electron multiplier tube used for detecting VUV radiation prevented us from carrying out experiments at higher gas pressures. Plasma was produced with a repetition rate of 4 Hz. The discharge duration was lengthened to 20 ms in the present experiment, since the rise times of the electron and neutral radical densities were longer in the C_4F_8 plasma than in the CF_4 plasma [the discharge duration of the previous CF_4 plasma was 10 ms (Ref. 16)].

Measurement of the F atom density was carried out in the downstream plasma at a distance of approximately 50 cm from the end of the helical antenna. The wavelength of the probe emission for detecting F atoms at the ground state ($2p^5\,{}^2P^0$) was 95.85 nm, which was obtained from a compact ECR CF_4 plasma device operated with a low microwave

[a]Electronic mail: sasaki@nuee.nagoya-u.ac.jp

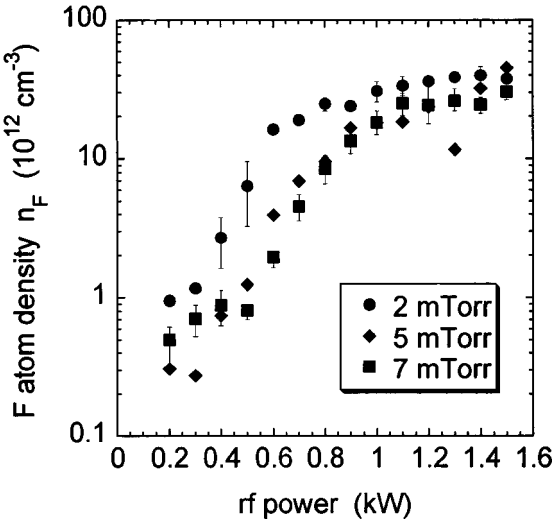

FIG. 1. Absolute F atom density measured by vacuum ultraviolet absorption spectroscopy as a function of the rf power for C_4F_8 gas pressures of 2, 5, and 7 mTorr.

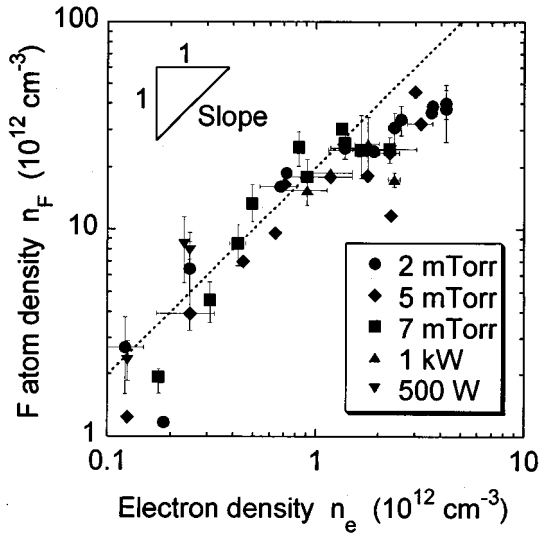

FIG. 2. The F atom density is plotted as a function of the electron density for fixed gas pressures of 2, 5, and 7 mTorr and for fixed rf powers of 0.5 and 1 kW, respectively. The electron density was varied by changing the rf power and the gas pressure. The dotted curve represents the relationship $n_F \propto n_e$.

power (0.1 kW) and a low gas pressure (1 mTorr). The ECR plasma device (light source) and the helicon-wave plasma source were connected by a windowless vacuum tube since window materials cannot transmit optical emission below 100 nm. Differentially pumping the vacuum tube prevented neutral species from passing between the helicon and the ECR plasmas. The VUV emission was detected using a VUV monochromator and an electron multiplier tube. The pressures in the monochromator and the electron multiplier tube were kept below 8×10^{-5} Torr by two-stage differential pumping. The absorption length of 36 cm, which was determined by two stainless-steel plates with orifices for differential pumping, was much longer than the diameter (3 cm) of the plasma column. A uniform distribution was assumed for the F atom density in the helicon chamber since the lifetime of F atoms was much longer than the geometrical diffusion time determined by the chamber design. The absolute F atom density was deduced by using the conventional theory[19] and by assuming Doppler broadening at a temperature of 400 K for spectral distribution of the probe emission. Doppler broadening at 300 K was assumed for the spectral distribution of absorbing F atoms in the helicon chamber since most of the F atoms were located outside the plasma column. The rotational temperature of the CF radicals, which was determined from the excitation spectrum in the LIF measurements, was 300–380 K in the plasma column. If we assume a temperature of 400 K for absorbing F atoms, then changes in the absolute F atom densities shown in this article are within a factor of 1.5. A more detailed description of VUVAS will be presented elsewhere. The electron density of the plasma was measured using a microwave interferometer (35 GHz) located 10 cm upstream from the observation chord for VUVAS.

III. RESULTS AND DISCUSSION

A. Absolute F atom density

Figure 1 shows the absolute density of F atoms in the helicon-wave C_4F_8 plasma as a function of the rf power for gas pressures of 2, 5, and 7 mTorr. The F atom densities plotted in Fig. 1 were observed at a discharge time of 19.9 ms, 0.1 ms before termination of the rf power. The measurements were repeated two to three times for the same rf power, and the average F atom density for each rf power is plotted in Fig. 1. The error bars represent the maximum and minimum values. The F atom density was 3×10^{11}–5×10^{13} cm^{-3} for rf powers of 0.2–1.5 kW. The F atom density in the CF_4 plasma produced in the same machine ranged from 9×10^{11} to 2×10^{13} cm^{-3} for similar rf powers and gas pressures.[16] Although the F atom density in the C_4F_8 plasma was of the same order as that in the CF_4 plasma, the densities of CF_x ($x=1,2$) radicals were one order higher in the C_4F_8 plasma.[12,13] In other words, the density ratio of CF_x radicals to F atoms was improved considerably. The dissociation degree of the parent gas was higher in the C_4F_8 plasma than in the CF_4 plasma. The electron density was lower for higher gas pressures, which resulted in lower F atom densities as shown in Fig. 1. This tendency was also observed in the CF_4 plasma,[16,20] and is probably due to the decrease of the excitation efficiency of the helicon wave.[21]

The F atom density shown in Fig. 1 is plotted again in Fig. 2 as a function of the electron density. In Fig. 2, results obtained by another operation are added; the F atom densities were also measured for various gas pressures with fixed rf powers of 0.5 and 1 kW. As seen from Fig. 2, the F atom density range is one order higher than the electron density. A linear relationship was found between the electron and F atom densities for electron densities lower than 1.5×10^{12} cm^{-3}. The dotted curve represents the relationship $n_F \propto n_e$. For electron densities higher than 1.5×10^{12} cm^{-3}, the F atom density was slightly saturated.

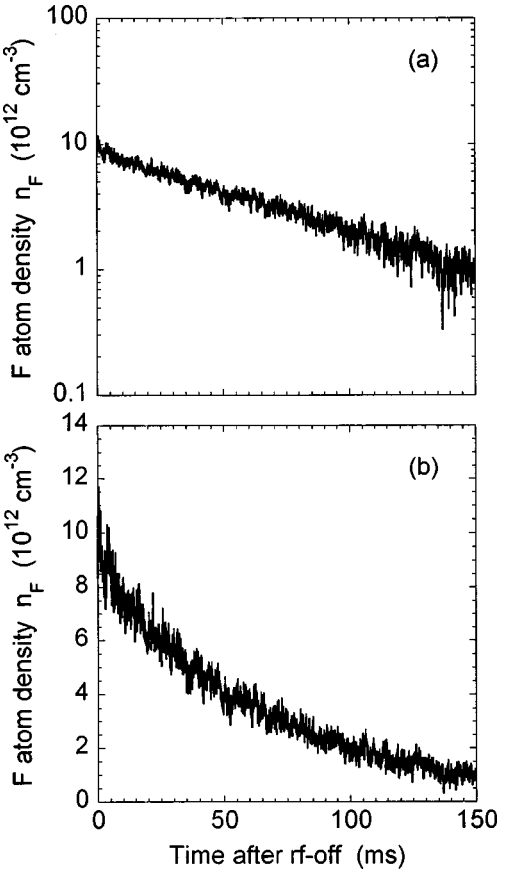

FIG. 3. Logarithmic (a) and linear (b) plots of the temporal variations of the F atom density in the afterglow for a gas pressure of 2 mTorr. The rf power was 1 kW.

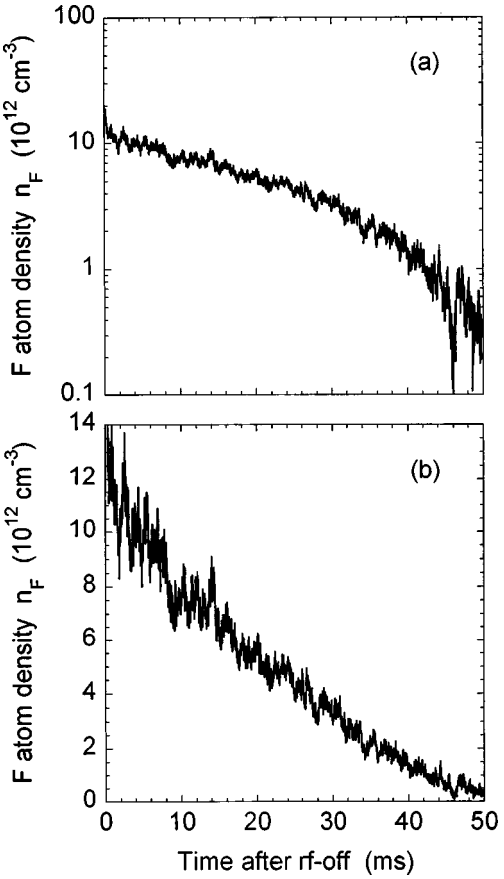

FIG. 4. Logarithmic (a) and linear (b) plots of the temporal variations of the F atom density for a gas pressure of 7 mTorr. The rf power was 1 kW.

Figure 1 shows a steep (nearly exponential) increase in the F atom density for rf powers in the range 0.2–0.7 kW. The increase in the electron density is also steep since it is proportional to the F atom density, as shown in Fig. 2. These results imply that the dissociation and ionization efficiencies increase rapidly with rf power in the C_4F_8 plasma. This increased efficiency is attributed partly to a change in the composition of the positive ion species. Positive ions are composed mostly of molecular ions (CF_x^+) for the low-density condition, but the fractional abundance of atomic ions (C^+ and F^+) increases with the electron density.[20] The rate constants of recombination with electrons are much smaller for atomic ions than for molecular ions. Hence the increase in the electron density reduces the loss rate of electrons through a change in the composition from molecular ions to atomic ions, resulting in the steep increase in the dissociation and ionization efficiency observed experimentally.[20]

B. Lifetime measurements

In order to examine the loss processes of F atoms in a high-density C_4F_8 plasma, the temporal variation of the F atom density was measured in the afterglow. Figures 3 and 4 show typical temporal variations of the F atom density for a rf power of 1 kW and C_4F_8 pressures of 2 and 7 mTorr. The origins of the horizontal axes correspond to the termination of the rf power. The vertical axes are represented by logarithmic and linear scales. For low gas pressures such as 2 mTorr, the F atom density decreased exponentially as shown in Fig. 3(a), while for higher gas pressures such as 7 mTorr, considerable deviation from the exponential curve was observed in the late afterglow ($t>30$ ms) as shown in Fig. 4(a). In this case, the decrease in the F atom density was nearly linear with respect to time as shown in Fig. 4(b). The linear decrease implies that the loss rate of F atoms is not affected by the gas-phase density.

As shown in Figs. 3 and 4, exponential and linear decreases were observed in the temporal variation of the F atom density in the afterglow. Therefore for simplicity, we have assumed two decay processes in the rate equation analysis: exponential-decay (first-order kinetics) and linear-decay (zero-order kinetics) components. Since the production of F atoms in the afterglow is negligible, the temporal variation of the F atom density can be analyzed by the following rate equation,

$$\frac{dn_F(t)}{dt} = -\frac{n_F(t)}{\tau} - \xi, \tag{1}$$

where τ is the time constant of the exponential-decay component and ξ denotes the constant reaction rate of the linear-decay component. Equation (1) can be solved easily, and its solution is

$$n_F(t) = (n_{F0} + \tau\xi)\exp\left(-\frac{t}{\tau}\right) - \tau\xi, \tag{2}$$

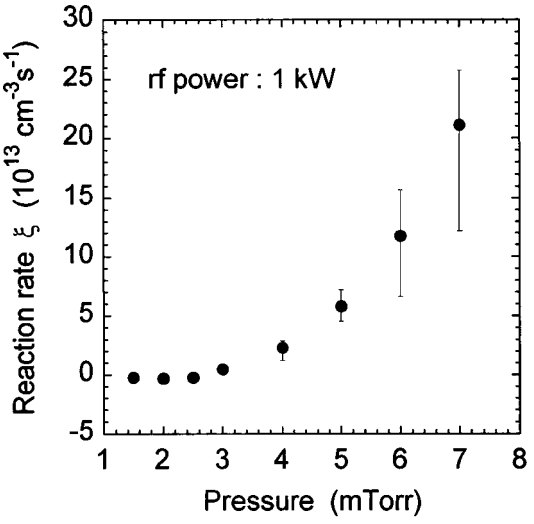

FIG. 5. The reaction rate ξ of the linear (constant-rate) decay component as a function of the C_4F_8 gas pressure.

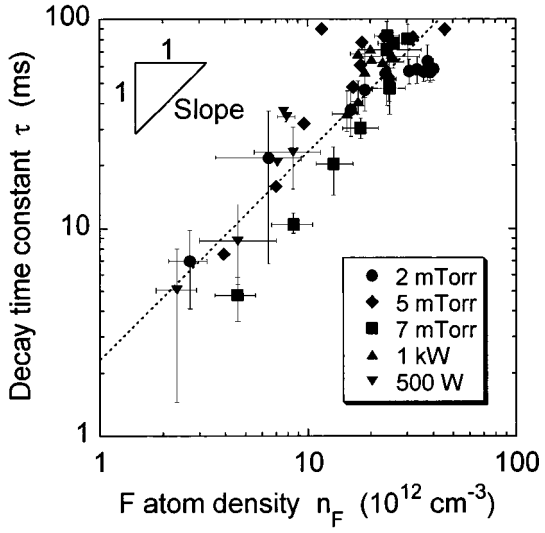

FIG. 6. The time constant τ of the exponential-decay component as *s* function of the F atom density just before termination of the rf power. The dotted curve represents the relationship $\tau \propto n_F$.

where n_{F0} is the F atom density just after termination of the rf power. Equations (1) and (2) are valid for $n_F(t) \leqslant 0[t \geqslant t_0 = \tau \ln(1+n_{F0}/\tau\xi)]$. We were able to fit all of the experimental observations of the temporal variation of the F atom density to Eq. (2) with minimum scatter. The time constant τ and the reaction rate ξ were thus evaluated from the experimental observations.

The pressure dependence of the reaction rate ξ for a fixed rf power of 1 kW is shown in Fig. 5. The condition $\xi=0$ corresponds to an exponential decrease. The reaction rate ξ was strongly dependent on the C_4F_8 pressure, but was roughly independent of rf power. An exponential curve fits the temporal variation of the F atom density well for gas pressures lower than 3 mTorr. For higher gas pressures, the reaction rate of the linear-decay component increases considerably. Reaction rates larger than 10^{14} $cm^{-3}\,s^{-1}$ were observed for gas pressures higher than 6 mTorr. In these cases, the F atom density decreased almost linearly with respect to time.

The time constant τ of the exponential-decay component was dependent on both the rf power and the gas pressure. A longer decay time constant was observed for higher rf powers and the lower gas pressures. This means that high-density discharges result in longer F atom lifetimes in the afterglow. The most meaningful graph for τ is obtained when it is plotted as a function of the F atom density just before termination of the rf power. As shown in Fig. 6, all the experimental results roughly converge to a proportional relationship between τ and n_F, even though both the rf power and the gas pressure had wide ranges of 0.2–1.5 kW and 2–7 mTorr, respectively. The dotted curve shown in Fig. 6 represents the relationship $\tau \propto n_F$.

C. Loss processes of F atoms

The loss of F atoms by gas-phase reactions should obey second-order kinetics since there are probably no species that have a density much higher than the F atom density. Therefore, the exponential decrease (first-order kinetics) of the F atom density may not be due to any gas-phase reactions. Undoubtedly, the linear (constant-rate) decrease (zero-order kinetics) cannot also be explained by gas-phase reactions. The experimentally observed lifetimes of F atoms are much longer than the geometrical diffusion time constant (~0.2–0.4 ms) determined by the chamber design.[22] Hence, both decay processes are probably surface reactions on the chamber wall. In other words, the two surface processes are active simultaneously in the afterglow.

The total number of F atoms lost by the two decay processes per unit volume can be evaluated with Eqs. (1) and (2). Due to the exponential-decay process, the number of F atoms that disappears in the afterglow is given by

$$n_{F1} = \int_0^{t_0} \frac{n_F(t)}{\tau} dt = n_{F0} - \xi\tau \ln\left(1+\frac{n_{F0}}{\xi\tau}\right), \tag{3}$$

while the number of F atoms lost by the linear-decay process is given by

$$n_{F2} = \int_0^{t_0} \xi dt = \xi t \ln\left(1+\frac{n_{F0}}{\xi\tau}\right), \tag{4}$$

where time t_0 is well defined by $n_F(t_0)=0$. Figure 7 shows the partial fraction of the two decay processes, defined by n_{F1}/n_{F0} and n_{F2}/n_{F0}, as a function of the C_4F_8 gas pressure. As is shown, the contribution of the linear-decay component increases with the gas pressure. For gas pressures higher than 6 mTorr, the linear-decay component dominates the exponential component in the total number of F atoms lost in the afterglow.

The exponential decrease is a typical feature of simple diffusion loss to the chamber wall. On the other hand, the constant-rate decrease is an unknown process, and is not understood well. Under the assumption of Langmuir kinetics, the adsorption flux of F atoms to the chamber wall is given by[23]

$$\Gamma_{ads} = K_a n_{FS} n_0' (1-\theta), \tag{5}$$

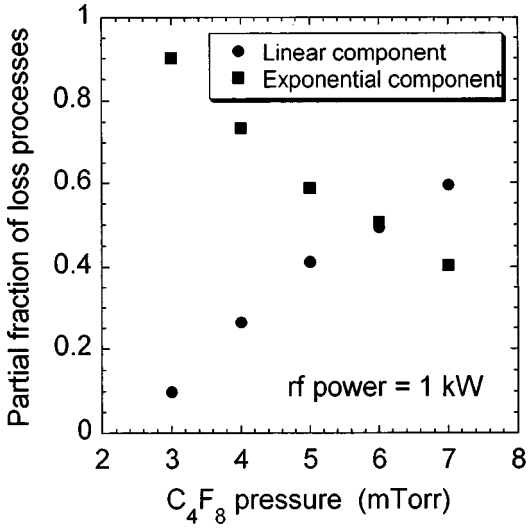

FIG. 7. The partial fraction of the exponential- and linear-decay components given by n_{F1}/n_{F0} (square) and n_{F2}/n_{F0} (circle), respectively, as a function of the C_4F_8 gas pressure.

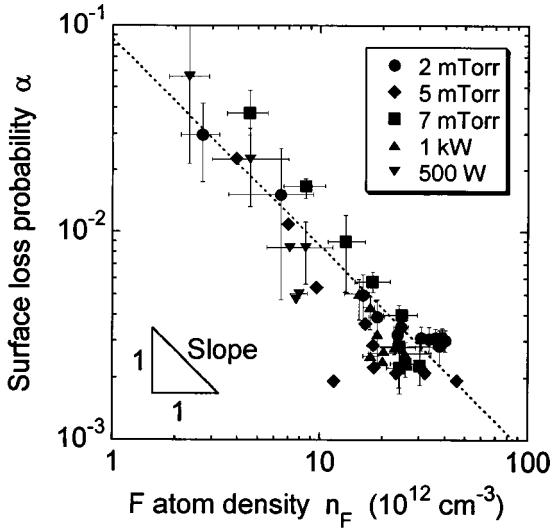

FIG. 8. The surface loss probability corresponding to the decay time constant τ as a function of the F atom density just before termination of the rf power. The dotted curve represents the relationship $\alpha \propto n_F^{-1}$.

where n_{FS} is the gas-phase F atom density at the surface, n_0' denotes the area density of adsorption sites contributing to the linear-decay process, and K_a is the rate coefficient. The surface coverage θ (the fraction of sites covered with adsorbate) is evaluated as[23]

$$\theta = \frac{Kn_{FS}}{1+Kn_{FS}}, \tag{6}$$

where $K = K_a/K_d$ with K_d being the rate coefficient for desorption. According to Eqs. (5) and (6), we obtain $\Gamma_{ads} \simeq K_d n_0'$ with $1-\theta \simeq 1/Kn_{FS}$ when $K_a n_{FS} \gg K_d$. This situation corresponds to a surface coverage close to unity. With a large surface coverage, it is possible that the adsorption rate is independent of the F atom density in the gas phase. However, this situation is probably uncommon in low-pressure discharges;[23] further investigation is needed to understand this surface reaction with zero-order kinetics.

It is noted again that there is also an ordinary surface reaction with first-order kinetics. A simple explanation for the simultaneous existence of the two surface processes is that the two reactions occur at different places on the chamber wall (e.g., the end plate of the chamber is bombarded intensely by positive ions, compared to the side wall of the cylindrical vessel). However, the strong pressure dependence of the partial fraction of the two processes shown in Fig. 7 is difficult to understand from the above explanation. At the present time, we believe there are two types of reaction sites on the wall, which is covered with fluorocarbon polymer films produced by the high-density C_4F_8 plasma. The difference in the reactivity may be due to a difference in the chemical composition at the sites.

A comparison of the instantaneous reaction rates shows that the exponential-decay component dominates the linear-decay component in the early afterglow since n_F remains high ($n_F/\tau \gg \xi$). If the exponential-decay component represents simple diffusion loss to the chamber wall, the time constant τ is related to the surface loss probability α by[24]

$$\tau \simeq \frac{2l_0(2-\alpha)}{\bar{v}\alpha}, \tag{7}$$

where, $\bar{v}$ is the mean velocity of the F atoms, given by $\sqrt{8kT/\pi M}$. (T and M are the temperature and mass of the F atoms, respectively, and k is the Boltzmann constant), and $l_0 = V/S$ with V and S being the volume and surface area of the chamber, respectively. This equation is accurate for surface loss probabilities much smaller than unity, which correspond to the F atom lifetimes much longer than the geometrical diffusion time. The surface loss probability in the early afterglow was evaluated from τ with Eq. (7). Figure 8 shows the surface loss probability α as a function of the F atom density just before termination of the rf power. As is shown in Fig. 8, α varies inversely with n_F. The dotted curve represents the relationship $\alpha \propto n_F^{-1}$. This result is understood as an increase in the surface coverage for higher F atom densities, resulting in a smaller surface loss probability.[25] The surface loss probability is a decreasing function of the coverage.[23] It is noted that the surface loss probability of F atoms in a CF_4 plasma produced in the same machine was on the order of 10^{-3}. It was strongly dependent on the gas pressure but was roughly independent of the rf power.[16]

IV. CONCLUSIONS

In conclusion, we have shown the following.

(1) We have carried out absolute density measurements of F atoms in low-pressure, high-density c-C_4F_8 plasmas by vacuum ultraviolet absorption spectroscopy.
(2) The F atom densities were on the order of 10^{11}–10^{13} cm^{-3} for rf powers of 0.2–1.5 kW and gas pressures of 2–7 mTorr.
(3) The F atom density was roughly proportional to the electron density for $n_e \leqslant 1.5\times10^{12}$ cm^{-3}. The absolute F atom density was one order higher than the electron density.

(4) Two decay processes (exponential and linear components) were found in the temporal variation of the F atom density in the afterglow.
(5) The time constant of the exponential-decay component was roughly proportional to the F atom density in the discharge phase.
(6) The surface loss probability corresponding to the time constant of the exponential-decay component was on the order of 10^{-3}–10^{-1}. The surface loss probability decreased inversely with the F atom density. This suggests that a higher F atom density in the discharge results in a larger coverage of the wall surface.
(7) The reaction rate of the linear-decay component was strongly dependent on the gas pressure, but was roughly independent of the rf power. The contribution of the linear-decay component was significant for high gas pressures.

ACKNOWLEDGMENTS

The authors would like to thank Dr. S. Kubota of Plasma Research Center, University of Tsukuba, for correcting the English. This work was supported by the Tatematsu Foundation and by a Grant-in-Aid for Scientific Research from the Ministry of Education, Science, Sports, and Culture of Japan.

[1] S. Matsuo and Y. Adachi, Jpn. J. Appl. Phys., Part 2 **21**, L4 (1982).
[2] T. Fukusawa, A. Nakamura, H. Shindo, and Y. Horiike, Jpn. J. Appl. Phys., Part 1 **33**, 2139 (1994).
[3] G. S. Oehrlein, Y. Zhang, D. Vender, and O. Joubert, J. Vac. Sci. Technol. A **12**, 333 (1994).
[4] S. Samukawa, Jpn. J. Appl. Phys., Part 1 **32**, 6080 (1993).
[5] T. Tsukada, H. Nogami, Y. Nakagawa, and E. Wani, Jpn. J. Appl. Phys., Part 1 **33**, 4433 (1994).
[6] S. Samukawa, Jpn. J. Appl. Phys., Part 1 **33**, 2133 (1994).
[7] M. Magane, N. Itabashi, N. Nishiwaki, T. Goto, C. Yamada, and E. Hirota, Jpn. J. Appl. Phys., Part 2 **29**, L829 (1990).
[8] H. Sugai and H. Toyoda, J. Vac. Sci. Technol. A **10**, 1193 (1992).
[9] J. P. Booth, G. Hancock, N. D. Perry, and M. J. Toogood, J. Appl. Phys. **66**, 5251 (1989).
[10] C. Suzuki and K. Kadota, Appl. Phys. Lett. **67**, 2569 (1995).
[11] K. Miyata, M. Hori, and T. Goto, J. Vac. Sci. Technol. A **14**, 2343 (1996).
[12] C. Suzuki, K. Sasaki, and K. Kadota, J. Appl. Phys. **82**, 5321 (1997).
[13] C. Suzuki, K. Sasaki, and K. Kadota, J. Vac. Sci. Technol. A (to be published).
[14] J. W. Coburn and M. Chen, J. Appl. Phys. **51**, 3134 (1980).
[15] Y. Kawai, K. Sasaki, and K. Kadota, Jpn. J. Appl. Phys., Part 2 **36**, L1261 (1997).
[16] K. Sasaki, Y. Kawai, C. Suzuki, and K. Kadota, J. Appl. Phys. **82**, 5938 (1997).
[17] K. Sasaki, Y. Kawai, and K. Kadota, Appl. Phys. Lett. **70**, 1375 (1997).
[18] T. Shoji, Y. Sakawa, S. Nakazawa, K. Kadota, and T. Sato, Plasma Sources Sci. Technol. **2**, 5 (1993).
[19] A. G. Mitchell and M. W. Zemansky, *Resonance Radiation and Excited Atoms* (Cambridge University Press, Cambridge, 1961), p. 92.
[20] K. Sasaki, K. Ura, K. Suzuki, and K. Kadota, Jpn. J. Appl. Phys., Part 1 **36**, 1282 (1997).
[21] K. P. Shamrai and T. B. Taranov, Plasma Phys. Controlled Fusion **36**, 1719 (1994).
[22] R. C. Reid, J. M. Prausnitz, and T. K. Sherwood, *The Properties of Gases and Liquids* (McGraw–Hill, New York, 1977).
[23] M. A. Lieberman and A. L. Lichtenberg, *Principles of Plasma Discharges and Material Processing* (Wiley, New York, 1994), Chap. 9.
[24] P. J. Chantry, J. Appl. Phys. **62**, 1141 (1987).
[25] J. Matsushita, K. Sasaki, and K. Kadota, Jpn. J. Appl. Phys., Part 1 **36**, 4747 (1997).